Section 8

Development of and advances in ocean, sea-ice, and wave modelling and data assimilation.

Upgrades to the NCEP's Real-Time and UnRestricted Mesoscale Analysis Systems for the Significant Wave Height

S. Flampouris[1], M. S. F. V. De Pondeca[1], R. Padilla – Hernandez[1] & J. R. Carley[2]

[1]IM Systems Group at NOAA/NCEP; [2]NOAA/NCEP/EMC; College Park, MD, USA
Email: stylianos.flampouris@noaa.gov

Introduction

The National Centers for Environmental Prediction (NCEP) provides weather guidance to the United States National Weather Service and consequently to their clients. The portfolio of operational products includes the Real Time Mesoscale Analysis (RTMA) and the UnRestricted Mesoscale Analysis (URMA) which provide hourly gridded analyses of surface (land and marine) meteorological variables, precipitation, and cloudiness for contiguous United States (CONUS), Alaska, Hawaii, Puerto Rico, and Guam [1]. Starting with version 2.6, the URMA provided significant wave height (SWH) analysis for the oceanic coasts of CONUS [2], and with version 2.7, the system was expanded to Alaska (AK), Hawaii (HI), and Puerto Rico (PR) domains [3].
This paper presents the upgrades concerning the SWH analysis for the next RTMA and URMA version, 2.8, for the existing domains. It also summarizes the expansion of the two systems to provide analysis of SWH to the Great Lakes and Guam.

Mesoscale Analysis of Significant Wave Height

RTMA and URMA are almost identical systems, both of them based on the community Gridpoint Statistical Interpolation (GSI) data assimilation system [4] and using the 2D-Var approach. More information on the current operational setups can be found in [5]. The analysis grid for all domains is 2.5km, except for AK (3km). The main difference between RTMA and URMA is that URMA runs six hours after the RTMA to ingest all the acquired observations. The current version (2.7) for the analysis of SWH has the following setup:

i. All the operationally available observations (from altimeters and in-situ) are assimilated.

ii. The background is provided by the operational multigrid wave prediction systems, based on the NWS WAVEWATCH III® model and is downscaled to the domains of the mesoscale analysis. The preprocessing is based on advanced scripting to fully utilize the wgrib2 [6] capabilities.

iii. The parameters (variance and correlation lengths) of the background error covariance function were estimated based on two years of analysis, and they are provided through external files.

Upgrades for the Mesoscale Analysis of Significant Wave Height

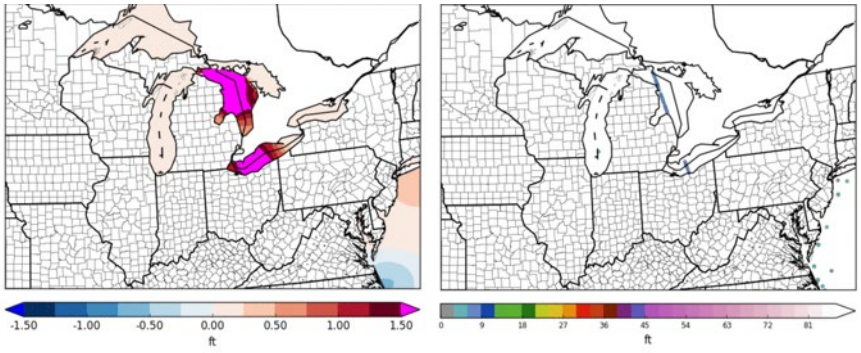

Figure 1. Increment (in ft) of significant wave height for the Great Lakes (left) and assimilated observations (right).

In the next version (2.8), the analysis systems have been upgraded as follows:

The URMA for CONUS includes SWH analysis for the Great Lakes (GL); the operational wave prediction system for the GL provides the background. Also, the operational surface ice analysis of NCEP is used to filter out the ice-covered sections of the Lakes. An example of the increment and the assimilated observations for the Great Lakes is shown in Figure 1.

The spatial resolution of all the analysis parameters for the PR domain will be doubled, from 2.5km to 1.25km. This upgrade does not have a statistically significant impact on the accuracy of the SWH analysis. Also, the option for assimilating observations from altimeters is activated; this upgrade has a limited effect on the analysis due to the satellite repeat cycle and the limited size of the domain.

Figure 2. Time series of bias, RMSE, and bias-corrected RMSE (BCRMSE), for the first guess (blue) and the analysis (red) at Guam.

An SWH analysis is added to the portfolio of the products for Guam. The default GSI values for global variance ($0.4m^2$) and horizontal correlation length (1.5 deg) for the SWH are used. The accuracy of the analysis is significantly higher in comparison to the background. But, as the in-situ observation locations are in shielded areas close to the coast of Guam, the spatial assimilation effect is minimal. Still, the assimilation of altimeter observations in the open ocean on the west side of the domain improves the nowcasting of the SWH significantly.

References

[1] Pondeca M., G. Manikin, G. DiMego, S. Benjamin, D. Parrish, J. Purser, W.-S. Wu, J. Horel, D. Myrick, Y. Lin, R. Aune, D. Keyser, B. Colman, G. Mann, and J. Vavra, 2011: The Real-Time Mesoscale Analysis at NOAA's National Centers for Environmental Prediction: Current Status and Development. Wea. Forecasting, 26, 593–612. DOI: http://dx.doi.org/10.1175/WAF-D-10-05037.1

[2] Flampouris S., J.-H. Alves, M. Pondeca, J. Whiting, 2016. Inclusion of significant wave height analysis to NCEP's UnRestricted Mesoscale Analysis (URMA), Research activities in atmospheric and oceanic modelling. Ed. E. Astakhova, WGNE,WCPR report no.15/2016,WMO

[3] Flampouris S., M. De Pondeca, J. Whiting, J. R. Carley, J.H. Alves, R. Yang, and S. Levine, 2018. Hourly Analysis of Significant Wave Height by the UnRestricted Mesoscale Analysis System at NCEP, Research activities in atmospheric and oceanic modelling. Ed. E. Astakhova, WGNE,WCPR report no.15/2018,WMO.

[4] Wu, W.-S., R. J. Purser, and D. F. Parrish, 2002: Three-dimensional variational analysis with spatially inhomogeneous covariances. Mon. Wea. Rev., 130, 2905–2916.

[5] Carley J. R., M. Pondeca, S. Levine, R. Yang, Y. Lin, S. Flampouris, J. Whiting, S. Melchior, A. M. Gibbs, R. J. Purser, B. T. Blake, G. Manikin, B. Yang, E. Colón, X. Zhang, M. T. Morris, M. Pyle, E. Rogers, and J. C. Derber, 2018: Ongoing Upgrades to NOAA's Real-Time Mesoscale Analysis System, 29th Conference on Weather Analysis and Forecasting (WAF)/25th Conference on Numerical Weather Prediction, 3-8 June 2018, Denver, CO.

[6] Ebisuzaki W. et al., 2017: WGRIB2; software available at http://www.ftp.cpc.ncep.noaa.gov/wd51we/wgrib2/.

RTOFS-DA: Real Time Ocean-Sea Ice Coupled Three Dimensional Variational Global Data Assimilative Ocean Forecast System

Zulema D. Garraffo[1,*], James A. Cummings[1], Shastri Paturi[1], Yan Hao[1], Dan Iredell[1], Todd Spindler[1], Bhavani Balasubramanian[1], Ilya Rivin[2], Hae-Cheol Kim[3], and Avichal Mehra[4]
[1]IMSG at NOAA/NWS/NCEP/EMC; [2]NOAA/NOS; [3]UCAR at NOAA/GFDL; [4]NOAA/NWS/NCEP/EMC
*Zulema.Garraffo@noaa.gov

Introduction

The operational Real Time Ocean Forecast System (RTOFS v1, Mehra et al., 2015) is initialized each day with ocean analyses produced daily at the Naval Oceanographic Office (Metzger et al., 2014). The core of this system consists of the coupled HYCOM and CICE numerical models, at 1/12 degree horizontal resolution with 41 layers on a global tri-polar grid. The ocean models are forced by GDAS/GFS forcing fields. In the upcoming upgrade of RTOFS (RTOFS v2), a multivariate, multi-scale 3DVar data assimilation is being added to RTOFS, which is referred to as RTOFS-DA. This new initialization capability is a coupled ocean and sea ice end-to-end system with data quality control, variational analysis and diagnostics. The analysis is performed directly on the HYCOM tri-polar grid layers using a 24-hour update cycle.

RTOFS-DA system

The daily RTOFS-DA cycle consists of several steps. The first step is decoding observational data from NetCDF or BUFR formatted input sources. The observations currently processed by RTOFS-DA include: (1) satellite and in situ Sea Surface Temperature (SST) from METOP-A, METOP-B, JPSS-VIIRS, NPP-VIIRS, GOES-16, HIMAWARI-8, ships, and buoys; (2) Sea Surface Salinity (SSS) from SMAP, SMOS, and buoys; (3) profiles of Temperature and Salinity from XBT, CTD, Argo floats, buoys, gliders, Alamo floats, animal-borne sensors, and Saildrone; (4) Absolute Dynamic Topography (ADT) from Jason, Cryosat, Altika, and Sentinel altimeters; (5) sea ice concentration from SSMI/S, AMSR2, and VIIRS; (6) surface velocity from HF Radar, ADCP, and drifting buoys; and (7) chlorophyll from ocean color (VIIRS, Sentinel). The system is designed to incorporate new observing systems, such as METOP-C, GOES-17, and HIMAWARI-9, as the data become available.

The second step is quality control (QC) of the observations in real-time using a fully automated system. The QC is done in stages incorporating sensibility, error and consistency checks. The QC outcomes are the likelihood that an observation contains an error, plus condition flags. All QC tests are performed before a QC decision is made on accepting, rejecting or scheduling the observation for correction. The QC decision-making algorithm resolves multiple background field checks (climate, cross validation analysis, and model forecasts). The QC error outcomes and condition flags are used to select valid observations for the assimilation.

The third step is forming the innovations (observation minus forecast) of validated observations within the synoptic time window of the assimilation (24-hours). This step includes application of various data thinning and data selection criteria to remove redundancies in the observations with respect to the HYCOM horizontal and vertical grid resolution. The high-density SST, SSS, and sea ice data are assimilated using the First Guess Appropriate Time (FGAT) method using innovations created from hourly HYCOM surface forecast fields. FGAT is used to prevent aliasing of the diurnal cycle in the analysis. Absolute Dynamic Topography (ADT) data are assimilated by first removing a HYCOM mean Sea Surface Height (SSH) bias with respect to the altimeter data. The correction is nearly constant (~50cm) for each altimeter track and for each altimeter satellite. ADT data assimilation adjusts HYCOM layer interface pressures by using a direct method (Cooper and Haines, 1996) that preserve model Temperature-Salinity relationships, with surface constraints provided by forecast SST, SSS, and mixed layer depths.

The fourth step is execution of the variational analysis system. The analysis takes on input innovations from randomly located observations and outputs increments, or corrections, on the HYCOM tri-polar grid layers. The increment fields include corrections to model prognostic variables not directly observed using multivariate relationships built into the analysis covariances (Cummings and Smedstad, 2013). The RTOFS-DA analysis increments are then added to the 24-hr forecast fields in the HYCOM restart file using a 3-hourly Incremental Analysis Update (IAU) procedure.

Simulation Results

A simulation that started on 23 August 2019 continues to the present in near real time. The global horizontally averaged vertical sections (Figure 1) for temperature bias (Observations-Forecast, O-F) show a maximum of 0.5°C at the depth of the seasonal thermocline (~150m) and a negative bias (-0.2°C) at the depth of the permanent thermocline (~800m). The maximum salinity bias is approximately 0.02 PSU at 150m. The residuals (Observation-Analysis, O-A) are essentially zero, which indicates that RTOFS-DA is effective at extracting all of the information contained in the observations.

RTOFS-DA Florida Current transports (Figure 2) show good agreement with observations and operational RTOFS during the time period of Hurricane Dorian, with a sharp decrease in transport due to the hurricane-force winds (08/31/19 – 09/07/19).

RTOFS-DA ocean heat content (OHC) for the same period was compared to the NESDIS product (not shown) with very similar distributions of OHC and 26°C isotherm topography. SST cooling in the wake of the hurricane, however, was not present in the NESDIS product. Surface drifter tracks (not shown) verify the positions of the Kuroshio, Gulf Stream, and Agulhas Current fronts and corresponding ocean circulation features in the HYCOM SSH forecast fields.

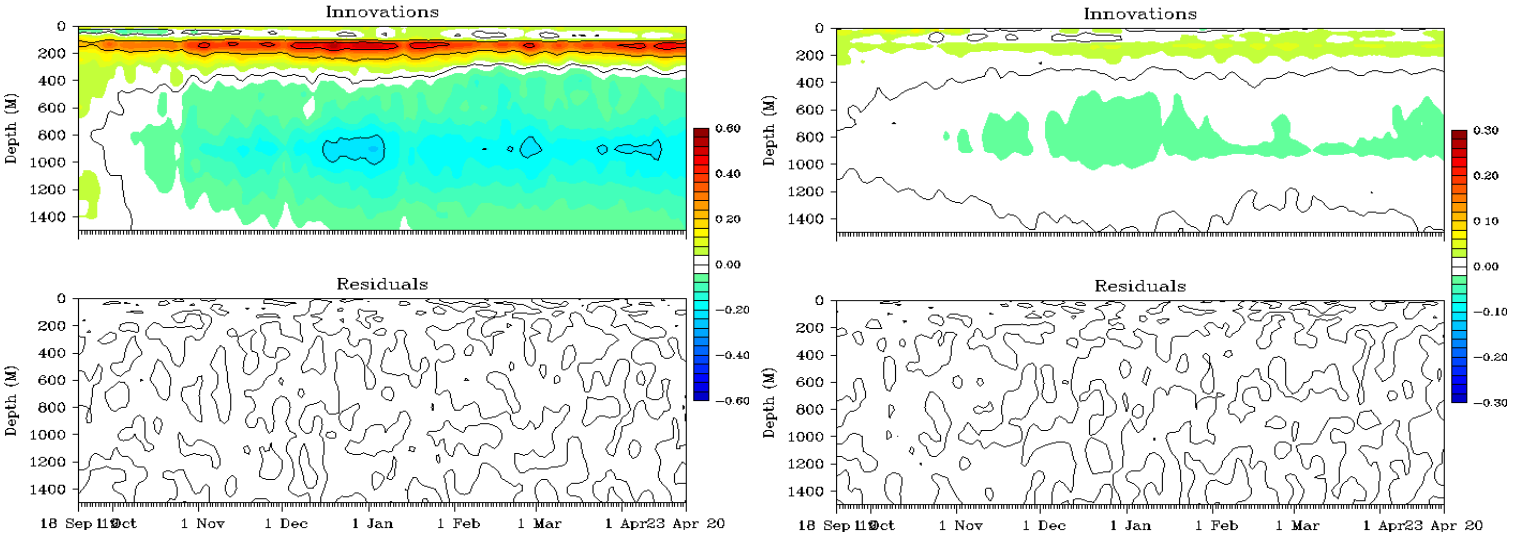

Figure 1: Horizontally averaged vertical sections of Temperature (left) and Salinity (right) innovations (O-F) and residuals (O-A) from 18 September 2019 through 23 April 2020.

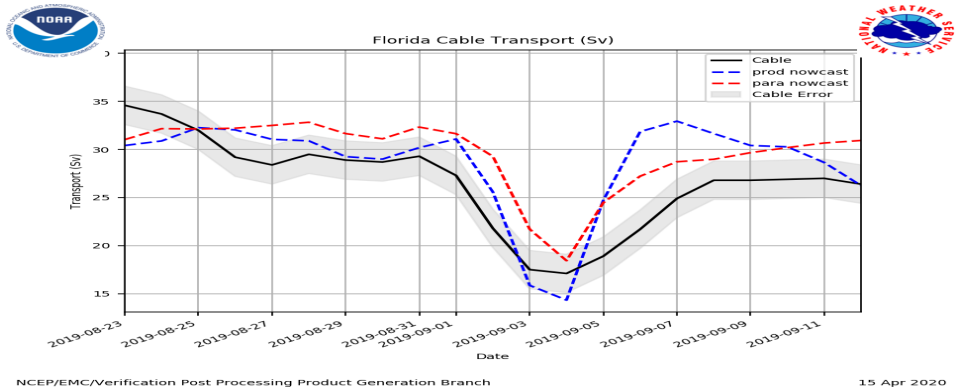

Figure 2:
Florida Current transports from RTOFS-DA (in red) compared with those from cable observations (in black) and operational RTOFS (in blue).

References

Cooper M. and Haines KA, 1996. Altimetric assimilation with water property conservation. J. Geophys Res 24, 1059-1077

Cummings, J. A. and O. M. Smedstad. 2013. Variational Data Assimilation for the Global Ocean. Data Assimilation for Atmospheric, Oceanic and Hydrologic Applications (Vol II) S. Park and L. Xu (eds), Springer, Chapter 13, 303-343.

Mehra, A.; I. Rivin; Z. Garraffo; B. Rajan, 2015. Upgrade of the Operational Global Real Time Ocean Forecast System, 2015. In: Research Activities in Atmospheric and Oceanic modeling, Ed. Askathova, WMO/World Climate Research Program Report No.12/2015. http://bluebook.meteoinfo.ru/uploads/2015/chapters/BB_15_s8.pdf

Metzger, E.J; O.M. Smedstad; P.G. Thoppil; H.E. Hurlburt; J.A. Cummings; A.J. Wallcraft; L. Zamudio; D.S. Franklin; P.G. Posey; M.W. Phelps; P.J. Hogan; F.L. Bub; and C.J. DeHaan, 2014. US Navy Operational Global Ocean and Arctic Ice Prediction Systems. *Oceanography* 27(3):32–43 http://dx.doi.org/10.5670/oceanog.2014.66

Overview of Sea Ice Data Assimilation Activities and System Development at NOAA-NCEP

Jong Kim[1], Guillaume Vernieres[2], and Stylianos Flampouris[1]

[1] IMSG/NOAA-NWS-NCEP-EMC, [2] UCAR-JCSDA/NOAA-NWS-NCEP-EMC

e-mail: jong.kim@noaa.gov

As Earth-observing systems continuously evolve, various data assimilation methodologies and algorithms have been exploited to make better use of observation data and computational resources. Under a joint effort for data assimilation integration (JEDI) at the Joint Center for Satellite Data Assimilation (JCSDA) and the National Centers for Environmental Prediction of the National Ocean and Atmospheric Administration (NOAA-NCEP), a seaice-ocean coupled assimilation system (SOCA) of the Modular Ocean Model version 6 (MOM6, https://www.gfdl.noaa.gov/mom-ocean-model) and the Community Ice Code version 5 (CICE5, https://github.com/CICE-Consortium/CICE) are integrated into the hybrid Global Ocean Data Assimilation System (GODAS) for new operational applications. We summarize the seaice data assimilation activity in the GODAS project with a brief introduction of the JEDI frame work.

In the JEDI software structure, an object oriented prediction system (OOPS) provides a core framework of algorithms that combine generic building blocks for data assimilation application algorithms. The object-oriented programming approach of the OOPS system, mostly written by C++, does not require knowledge of actual implementations of specific application model structures or observation data information. In the JEDI interface-based programming method, application calls are made with a list of the pre-defined OOPS abstract interfaces, rather than by direct calls of any unitary application routines or classes. A few articles (Trémolet, 2020, Holdaway et al., 2020, Honeyyager et al., 2020) introduce a key concept of the JEDI software system, to highlight how different data assimilation systems can be seamlessly established through the same software infrastructure and components. As a core JEDI application project, the SOCA data assimilation system has been implemented with the interface classes of Geometry, State, Increment, Model, LinearModel, and VariableChange. A C++ traits technique is applied to connect the SOCA application interfaces to the OOPS abstract interfaces and generic algorithms. In addition to developing the MOM6-CICE5 model interfaces, generic marine observation operators and data handling capabilities of the JEDI unified observation (forward) operator (UFO) and interface for observation data access (IODA) systems are also utilized in the SOCA project. The SOCA model interfaces have mainly been built for a coupled data assimilation system of MOM6-CICE5 [4,5]. However, a SOCA-CICE6 system has been demonstrated for a standalone data assimilation capability in CICE version 6 as well. The SOCA interfaces have been tested with a combination of variational and ensemble data assimilation cases: 3DVar, 3DEnVar, and 3D-FGAT and their hybrid variants. A high-resolution 1/4 degree cycled experiment has been conducted with an extensive set of observation data: see details in the paper (Holdaway et al., 2020). More information about the SOCA system is available at https://www.jcsda.org/jcsda-project-soca.

When a broad range of marine observation data sets are used to set initial conditions of the MOM6-CICE5, the SSMI seaice concentration data from DMSP F-15 (https://polar.ncep.noaa.gov/seaice/Analyses.shtml) is also utilized to set the initial conditions of the seaice category concentration variable of the CICE model. As ocean and sea ice are thermodynamically coupled, assimilation of seaice concentration data clearly serves as a good test case for assessing the benefits of a strongly coupled SOCA data assimilation system over weakly coupled data assimilation cases. Here we summarize a preliminary experimental result of the SOCA system of using seaice concentration data. The experiment was done using 3DVar and a 24-hour assimilation window. During the experiment, various observation filters of the JEDI UFO system were applied: bounds check, background check, and thinning. Figure 1

shows seaice concentration analysis and increment (analysis-minus-background) fields obtained from the test of the hybrid GODAS system for the assimilation of the SSMI observation data. The assimilation process produces positive and negative increments in different areas. A positive increment to model background is a dominant feature in the Weddell Sea and Ross Sea. Negative increment is found over a broad range of the seaice boundary in the Southern Ocean. At this stage, we are not systematically applying a post-processing tool for quantification of analysis verification. However, we are still able to observe that analysis and increment fields produced from the experiment match well with patterns in the observation data. A few articles (Barth et al. 2015, Massonet et al., 2015) note that bias can be introduced with the data assimilation approach of multi-category seaice variables with aggregated ice observation data. As the GODAS system evolves, our priority will be focused on the scientific benefits of the SOCA-based data assimilation system with systematically tuned experiment sets.

The JEDI-based data assimilation framework and applications continuously evolve to be adopted for both existing and emerging operational data assimilation systems. With the recent release of the SOCA, MOM6, and CICE5/6 interfaces to NOAA-NCEP, future efforts will be focused on replacing the variational component of the current GODAS system with SOCA. In doing so, important aspects of the SOCA system to be investigated in the coming months are tuning up cycled experiments with robust quality control of observation data, verification of assimilation results with robust post-processing tools, and improving the system efficiency with a hybrid 3DVar and 3DEnVar approach.

References

Barth, A., Canter, M., Van Schaeybroeck, B., Vannitsem, S., Massonnet, F. and co-authors. 2015. Assimilation of sea surface temperature, sea ice concentration and sea ice drift in a model of the Southern Ocean. Ocean Model. 93, 22–39.

Holdaway, D., Vernières G., Wlasak M., and King S., 2020: Status of Model Interfacing in the Joint Effort for Data assimilation Integration (JEDI). JCSDA Quarterly, 66, Winter 2020.

Honeyager, R., Herbener, S., Zhang, X., Shlyaeva, A., and Trémolet, Y., 2020: Observations in the Joint Effort for Data assimilation Integration (JEDI) - UFO and IODA. JCSDA Quarterly, 66,

Massonnet, F., Fichefet, T. and Goosse, H. 2015. Prospects for improved seasonal Arctic sea ice predictions from multivariate data assimilation. Ocean Model. 88, 16–25.

Trémolet, Y., 2020: Joint Effort for Data assimilation Integration (JEDI) Design and Structure. JCSDA Quarterly, 66, Winter 2020.

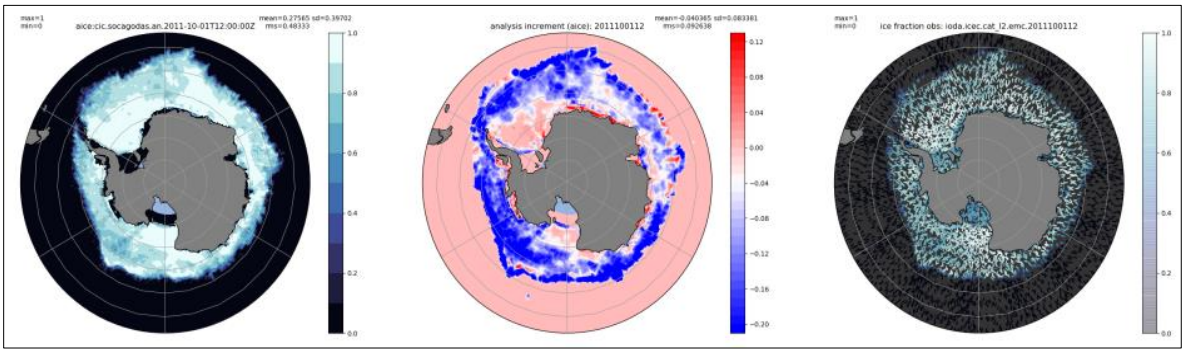

Figure 1: Seaice concentration analysis (left) and increment (middle) fields produced from a data assimilation experiment for the SSMI observation (right) data: 2011-10-01-12:00.

Changes of sea waves characteristics in the Arctic basin from model simulations for the 21st century

F.A. Pogarskiy[1] and I.I. Mokhov[1,2]

[1]A.M. Obukhov Institute of Atmospheric Physics RAS

[2]Lomonosov Moscow State University

pogarskiy@ifaran.ru, mokhov@ifaran.ru

The decrease in the sea ice extent in the Arctic basin in recent decades is accompanied by changes in sea waves. Here we analyze characteristics of wind waves activity in the Arctic basin using the WAVEWATCH III model (http://polar.ncep.noaa.gov/mmab/papers/tn276 /MMAB_276.pdf) simulations forced by wind and sea ice fields from simulations with the CMIP5 global climate models under different scenarios. Special attention is paid to the assessment of relative contribution of wind sea waves and swells to the total sea waves activity in the Arctic basin. Possible changes in the characteristics of sea waves characteristics are estimated by model simulations for the 21st century. Regional effects of interaction of wind sea waves and swells (chop-like events) are also estimated. Modeling was performed for the area north of 50°N with a spatial resolution of 1° in longitude and 0.5° in latitude. Both historical (1990-2005) and anthropogenic (RCP4.5 and RCP8.5 for the period 2006-2100) scenarios were used (see [1,2]).

The analysis of simulations with 11 models was carried out. Figures 1-3 present the results of simulations with the ACCESS1-3 and inmcm4 models with reasonable agreement with satellite data both regarding the location of sea ice boundaries in the Arctic basin and their changes over the recent decades.

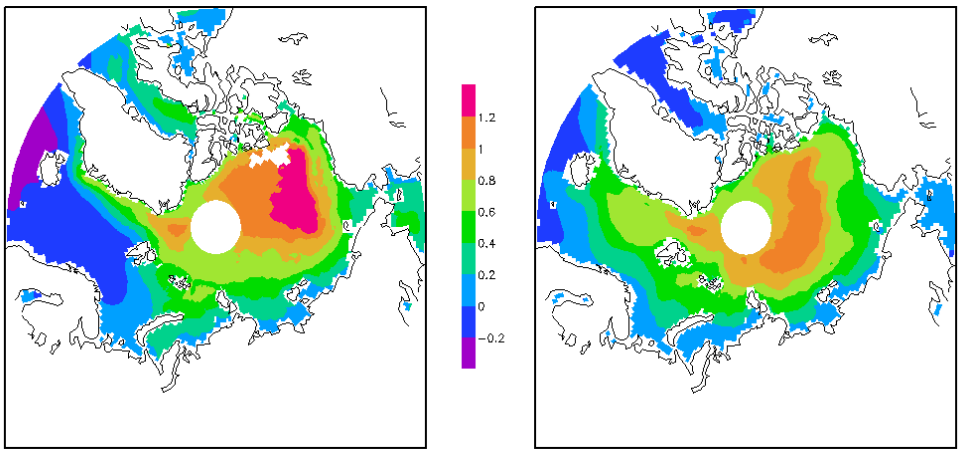

Figure 1. Changes in significant wave height (m) to the end of the 21st century (2091-2100) relative to the period 1990-2005 as simulated by WAVEWATCH III model with climate forcing from ACCESS1-3 (left) and inmcm4 (right) simulations under the RCP8.5 scenario.

According to the simulation results, a significant wave height and its extrema increase in different areas of the Arctic basin are related to a decrease in the sea ice extent (Fig. 1). The opposite tendency appears for the Atlantic sector of the Arctic basin with a reduction in wave height. These results based on simulations with global climate models under historical and RCP scenarios confirm previous results based on simulations with the regional model HIRHAM under SRES scenario [1].

Results of model simulations also demonstrate the complex response of swell sea waves in the Arctic Ocean to a combined effect of wind and sea ice forcings in a climate-change scenario during the 21st century (Fig. 2).

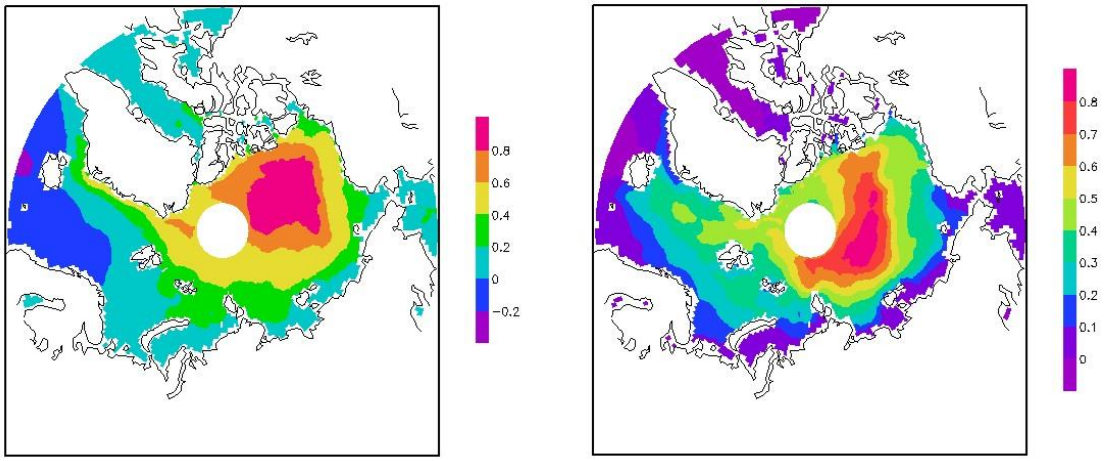

Figure 2. Changes in significant wave height of swell (m) to the end of the 21st century (2091-2100) relative to the period 1990-2005 as simulated by WAVEWATCH III model with climate forcing from ACCESS1-3 (left) and inmcm4 (right) simulations under the RCP8.5 scenario.

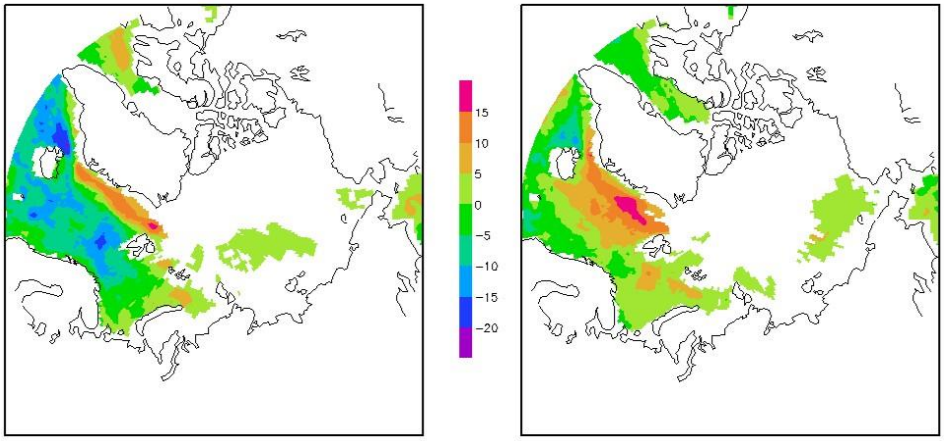

Figure 3. Changes in chop occurrence (number of cases per year) to the end of the 21st century (2091-2100) relative to the period 1990-2005 as simulated by WAVEWATCH III model with climate forcing from ACCESS1-3 (left) and inmcm4 (right) simulations under the RCP8.5 scenario.

According to the obtained results, the occurrence of chop-like events increases in the Greenland Sea and for different inner Arctic basin areas and decreases in the Norwegian Sea and the Barents Sea in the 21st century under RCP8.5 scenario (Fig. 3). Also, it is worth to note that model simulations show the general increase of the sea waves total energy in the Arctic basin in the 21st century for all months.

The analysis was carried out in the framework of the RSF project 19-17-00240. The analysis of changes in the sea waves characteristics due to the sea ice changes was carried out as part of the RFBR project 18-05-60111.

References

1. Khon V., Mokhov I.I., Pogarskiy F., Babanin A., Dethloff K., Rinke A., Matthes H. (2014) Wave heights in the 21 century Arctic Ocean simulated with a regional climate model. *Geophys. Res. Lett.*, **41** (8)**,** 2956-2961.
2. Khon V.C., Mokhov I.I., Semenov V.A. (2017) Transit navigation through Northern Sea Route from satellite data and CMIP5 simulations. *Environ. Res. Lett.*, **12,** 024010.

COVARIANCE FUNCTIONS IN MULTIVARIATE ASSIMILATION SYSTEM WITH ENSEMBLE KALMAN FILTER

V.N. Stepanov and Yu.D. Resnyanskii

Hydrometeorological Research Centre of Russian Federation (vlnst@hotmail.co.uk)

1. Introduction

The results of data assimilation systems substantially depend on the determination of the error covariances of the first guess field (ECFG) [1]. In oceanographic applications, primarily due to the effect of coasts on the dynamics of processes developing in the ocean, ECFGs are non-homogeneous and anisotropic functions [5]. In general, these functions contain a multivariate component that plays an important role. It is responsible for transferring observational information between model variables, which is crucial for extracting information about unobserved variables from directly observed variables.

2. Ensemble Kalman filter

One of effective ways to take into account the above-mentioned features of ECFG in sequential data assimilation schemes is the widely-used local ensemble transform Kalman filter (LETKF), which can be implemented with PDAF software product [2, 3]; http://pdaf.awi.de).

The authors [4] studied the properties of LETKF used with the NEMO model on the base of several examples assimilating synthetic data. The properties of the analysis procedure can be most clearly illustrated using single-observation experiments [5]. It is known that the analysis increments corresponding to single observations are proportional to the ECFG on which the analysis is based.

3. Model configuration

Here we present such illustrations for the LETKF assimilation system, which uses the 4-th version NEMO model (Nucleus for European Models of the Ocean) coupled with the thermodynamic sea ice model SI3. The model uses the ORCA1 configuration with a global grid resolution of 1×1° (362×332 grid nodes) and 75 vertical levels [4]. The parameters of the LETKF were set to the following values: the ensemble has $N = 20$ members, the forgetting factor $\rho = 0.95$, the observations are weighted by the 5th-order polynomial with an influence radius of $R = 3.5°$.

4. Single-observation experiments

In the examples under consideration, the assimilation procedure was fed with isolated single observations of different variables in the form of their deviations from the first guess field (usually called innovations). The structure of the increments resulting from the procedure's output gives a clear representation of the structure of the ECFG including its multivariate component. The Figure 1 shows the increments corresponding to innovations of sea level $\zeta = 10$ cm and of surface water temperature T_S=1°C located in different geographical areas. It is clearly seen that the structure of increments, and, consequently the ECFG, significantly depends on the geographical location.

There is also a close similarity between the shape of the sea level increments due to sea level innovations (Figure 1a) and to surface water temperature innovations (Figure 1b). This is explained by the fact that an increase in water temperature is accompanied by an increase in sea level ζ due to steric effects. For a typical value of the coefficient of thermal expansion of water $\alpha_T = 2{,}7\times10^{-4}$ K^{-1}, an increase in temperature by 1°C in the upper water layer of ~4 m corresponds to an increase of ζ by 1 cm that is in agreement with Figures 1a, b.

It should also be noted that in areas (regions 3, 4, 6, and 7 in Fig. 1b), where there are no significant temperature gradients or strong jet currents, the response to temperature changes reproduced by the assimilation system is weakly manifested, i.e., in regions with feeble dynamics, surface "delta-like observations" are weakened by the Kalman filter.

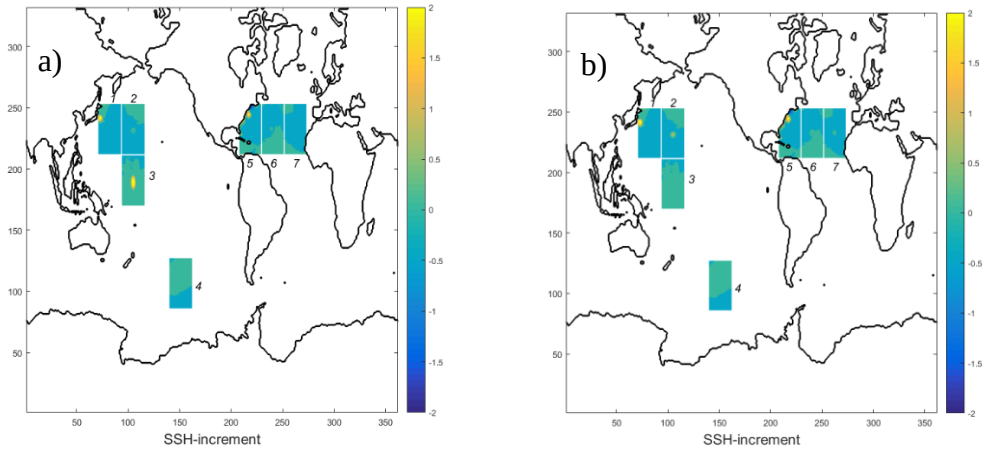

Figure 1. Sea level increments (in cm) corresponding to sea level innovations ζ = 10 cm (a) and surface water temperature innovations T_S = 1°C (b) located in seven different geographical regions.

Similar features can be seen in the vertical distributions of the increments of other variables (water temperature, salinity and horizontal components of the current velocity), corresponding to innovations in sea level and surface water temperature. Like horizontal distributions, the vertical structure is characterized by significant inhomogeneity seen in significant differences from region to region, and anisotropy, manifested in noticeable differences between zonal and meridional distributions.

These features are most distinct in dynamically active areas: in the Kuroshio (region 1) and Gulf Stream (region 5). Besides, excluding the western part of the equatorial Pacific, velocity increments in the open ocean are significant only in the upper layer (~100m), while these increments are noticeably significant near the coastal regions to a depth of ~1500m and to a depth of ~ 2000m in the equatorial Pacific.

Thus, the results of experiments assimilating single observations using the local ensemble Kalman filter (LETKF) in the NEMO ocean model demonstrate the perspective of using PDAF for the assimilation of observational data in the NEMO model.

References:

1. Daley R. Atmospheric data analysis. Cambridge University Press. Cambridge, New York: Cambridge University Press, 1991. 457 p. https://trove.nla.gov.au/version/45674382.
2. Nerger L., W. Hiller and J. Schröter, 2005: PDAF – The Parallel Data Assimilation Framework: Experience with Kalman filtering. Use of High Performance Computing in Meteorology: pp. 63–83.
3. Nerger, L., Hiller, W. (2013). Software for Ensemble-based Data Assimilation Systems - Implementation Strategies and Scalability. Computers and Geosciences, 55, 110–118. doi:10.1016/j.cageo.2012.03.026.
4. Stepanov V. N., Resnyanskii Yu. D., Strukov B. S., and Zelenko A. A. Evaluation of effects of assimilation of observed data in models of general ocean circulation by the Kalman ensemble filter method: numerical experiments with synthetic observations. Russian Meteorology and Hydrology. 2020. (in press).
5. Weaver A.T., Deltel C., Machu E., Ricci S., and Daget N. A multivariate balance operator for variational ocean data assimilation. Quarterly Journal of the Royal Meteorological Society. 2005. Volume 131, Issue 613. pp. 3605–3625. doi: 10.1256/qj.05.119.